

Local and nonlocal pressure Hessian effects in real and synthetic fluid turbulence

Laurent Chevillard,¹ Emmanuel Lévêque,¹ Francesco Taddia,¹ Charles Meneveau,² Huidan Yu,² and Carlos Rosales³

¹Laboratoire de Physique de l'École Normale Supérieure de Lyon, CNRS, Université de Lyon, 46 allée d'Italie F-69007 Lyon, France

²Department of Mechanical Engineering and Center for Environmental and Applied Fluid Mechanics, The Johns Hopkins University, 3400 N, Charles Street, Baltimore, Maryland 21218, USA

³Department of Mechanical Engineering, Technical University Federico Santa María, Avenida España 1680, Valparaíso 2340000, Chile

(Received 6 June 2011; accepted 19 August 2011; published online 21 September 2011)

The Lagrangian dynamics of the velocity gradient tensor \mathbf{A} in isotropic and homogeneous turbulence depends on the joint action of the self-stretching term and the pressure Hessian. Existing closures for pressure effects in terms of \mathbf{A} are unable to reproduce one important statistical role played by the anisotropic part of the pressure Hessian, namely the redistribution of the probabilities towards enstrophy production dominated regions. As a step towards elucidating the required properties of closures, we study several synthetic velocity fields and how well they reproduce anisotropic pressure effects. It is found that synthetic (1) Gaussian, (2) multifractal, and (3) minimal turnover Lagrangian map incompressible velocity fields reproduce many features of real pressure fields that are obtained from numerical simulations of the Navier Stokes equations, including the redistribution towards enstrophy-production regions. The synthetic fields include both spatially local, and nonlocal, anisotropic pressure effects. However, we show that the local effects appear to be the most important ones by assuming that the pressure Hessian is local in space, an expression in terms of the Hessian of the second invariant Q of the velocity gradient tensor can be obtained. This term is found to be well correlated with the true pressure Hessian both in terms of eigenvalue magnitudes and eigenvector alignments. © 2011 American Institute of Physics.

[doi:10.1063/1.3638618]

I. INTRODUCTION

The study of the velocity gradient tensor in fully developed turbulence has led to interesting findings and has contributed to improved understanding of many statistical and geometrical properties of turbulent flows. In particular, recent progress has been made in the study of the Lagrangian dynamics and modeling of the velocity gradient tensor (see Ref. 1 for an overview of the subject). This tensor is given by $A_{ij} = \partial u_i / \partial x_j$, where \mathbf{u} is the velocity vector. Taking a spatial gradient of the Navier-Stokes equations, the following transport equation for \mathbf{A} is obtained:

$$\frac{d\mathbf{A}}{dt} = -\mathbf{A}^2 - \mathbf{P} + \nu \Delta \mathbf{A}, \quad (1)$$

where d/dt stands for the Lagrangian time derivative, ν is the kinematic viscosity, and $P_{ij} = \partial^2 p / \partial x_i \partial x_j$ is the pressure Hessian. The first term $-\mathbf{A}^2$ is the self-stretching term. The restricted Euler (RE) approximation, which assumes an isotropic pressure Hessian $P_{ij} = -\text{tr}(\mathbf{A}^2) \delta_{ij} / 3$ and neglects viscous effects, leads to an autonomous set of coupled ordinary differential equations.² The intrinsic dynamics of the RE system leads to a finite time divergence of the components of \mathbf{A} during which the vorticity $\boldsymbol{\omega} = \nabla \wedge \mathbf{u}$ gets aligned with the eigenvector of the rate of strain, $\mathbf{S} = (\mathbf{A} + \mathbf{A}^\top) / 2$, associated with the intermediate eigenvalue, as often observed in real turbulence.^{1,3,4} To prevent the development of unphysical finite

time singularities, both the anisotropic part of the pressure Hessian and the viscous diffusion term have to be modeled. This was the subject of former works.⁵⁻⁷ In particular, closures were proposed in Ref. 7 for \mathbf{P} and $\nu \Delta \mathbf{A}$ in terms of the local value of \mathbf{A} . The local closures of Ref. 7, when inserted into the dynamics generated by Eq. (1) under the action of a stochastic forcing term, lead to stationary statistics of \mathbf{A} along Lagrangian trajectories which compare well with those obtained from direct numerical simulations (DNS) of the Navier-Stokes equations at moderate Reynolds numbers.⁸ At higher Reynolds numbers, predictions of the stochastic model proposed in Refs. 7 and 8 turn out to become unrealistic, mainly because of the weakness of the closure for the anisotropic part of the pressure Hessian.

Indeed, the pressure Hessian is related to the spatial distribution of the velocity gradient using singular integral operators⁹⁻¹³ according to

$$\frac{\partial^2 p}{\partial x_i \partial x_j} = -\text{tr}(\mathbf{A}^2) \frac{\delta_{ij}}{3} - \text{P.V.} \int k_{ij}(\mathbf{x} - \mathbf{y}) \text{tr}(\mathbf{A}^2)(\mathbf{y}) d\mathbf{y}. \quad (2)$$

In the above equation, the integral is understood as a Cauchy principal value (P.V.), and k_{ij} is the Hessian of the Green's function for the Laplacian operator, namely

$$k_{ij}(\mathbf{x}) = \frac{\partial^2}{\partial x_i \partial x_j} \frac{1}{4\pi|\mathbf{x}|} = \frac{|\mathbf{x}|^2 \delta_{ij} - 3x_i x_j}{4\pi|\mathbf{x}|^5}. \quad (3)$$

One can see from Eq. (2) that only the isotropic part of the pressure Hessian is purely local (the first term on the right-hand side (RHS) of Eq. (2)). All the nonlocal effects of pressure Hessian enter through the anisotropic part (or deviatoric part corresponding to the second term in the RHS of Eq. (2)). Hence, in this view, the RE approximation can be understood as the neglect of all the nonlocal effects implied by the incompressibility condition (or pressure field).

In order to quantify the precise action of pressure in numerical turbulent flows, it was proposed, in Ref. 8, to study the probability current associated with pressure in the plane spanned by the two highly relevant invariants of \mathbf{A} , R and Q (the so-called RQ -plane). One of these invariants, defined as

$$Q = -\frac{1}{2}\text{tr}(\mathbf{A}^2) = \frac{1}{4}|\omega|^2 - \frac{1}{2}\text{tr}(\mathbf{S}^2), \quad (4)$$

quantifies the net balance, or competition, between enstrophy and dissipation. The other important invariant, defined as

$$R = -\frac{1}{3}\text{tr}(\mathbf{A}^3) = -\frac{1}{4}\omega_i S_{ij} \omega_j - \frac{1}{3}\text{tr}(\mathbf{S}^3), \quad (5)$$

quantifies the competition between enstrophy production and strain skewness (i.e., dissipation production). As it will be recalled in the following, in terms of the velocity gradient evolution in statistically stationary turbulence, pressure has two important roles. First of all, pressure counteracts the development of the singularity implied by the self-stretching term. This feature is found to be well reproduced by existing closures.⁸ The other important pressure action is the redistribution of probabilities towards enstrophy production dominated regions (i.e., towards $R < 0$). This is not reproduced well by existing closures. As discussed in Refs. 8 and 14, a related deficiency of the closures is that they all predict that the pressure Hessian is proportional to Q . In the $R - Q$ plane dynamics, this implies that when $Q = 0$, the effect of pressure Hessian also vanishes. For real turbulence, there is no such vanishing of pressure Hessian effects when $Q = 0$.⁸

In this article, we investigate whether these particular features of pressure (redistribution of probabilities towards enstrophy production, and non-vanishing action even when $Q = 0$) are inherent to true Navier-Stokes turbulence or can also be observed in various approximations, namely synthetic turbulent velocity fields. Various types of synthetic fields are considered. The first type of synthetic field considered is Gaussian field obtained by superposing random-phase Fourier modes with prescribed spectra. The second type is called ‘‘multifractal’’¹⁵ and consists of a Gaussian field whose vorticity field is amplified by means of the ‘‘fluid deformation closure’’ and made consistent with multifractality’s long-range correlations in physical space.¹⁶ The third type of synthetic field is generated using the Lagrangian mapping technique.^{17,18} It also relies on random-phase Gaussian fields but then applies a multi-scale deformation of fluid particles using a simple Lagrangian mapping. For each of these synthetic velocity fields, a pressure field is obtained numerically by means of the pressure Poisson equation. As will be seen, unlike the local closures discussed above, these synthetic fields reproduce many correct

features of the pressure Hessian. In particular, they will be shown to reproduce the redistribution of probability towards enstrophy production, as well as displaying non-vanishing action, even when $Q = 0$.

The second part of the paper studies to what degree spatial locality is important in determining these properties of the anisotropic part of the pressure Hessian. As can be seen from the expression for the pressure Hessian (Eq. (2)), the anisotropic part of the pressure Hessian is also the part that is spatially nonlocal, i.e., the part that requires knowledge of $\text{tr}(\mathbf{A}^2)$ at positions $\mathbf{y} \neq \mathbf{x}$. Arguably, the more non-local effects are important, the more challenging it is to formulate closures in terms of local quantities. In order to examine the degree of locality, in the second part of this paper, we decompose the space integration in Eq. (2) into two parts: a local part given by the integration over a small ball of radius given by the Kolmogorov length scale η_K and the remainder being the ‘‘nonlocal’’ portion. We will show that neglecting the second non-local contribution leads to an expression that models the anisotropic part of the pressure Hessian in terms of the Hessian of the invariant Q . Using DNS data, this expression is compared with the true pressure Hessian.

II. PRESSURE HESSIAN FROM DNS AND SYNTHETIC VELOCITY FIELDS

A. Probability current in the RQ -plane

1. Definition of the probability current

We follow the approach used in Refs. 8 and 19, based on a Fokker-Planck equation for the dynamics of R and Q . To summarize the approach, we remark that it can be shown that the time evolution along a Lagrangian trajectory of the non-dimensional invariants $R^* = R/\sigma^3$ and $Q^* = Q/\sigma^2$ is given by

$$\frac{dQ^*}{dt^*} = -3R^* - \frac{1}{\sigma^3} A_{ik} H_{ki}^p - \frac{1}{\sigma^3} A_{ik} H_{ki}^v, \quad (6)$$

$$\frac{dR^*}{dt^*} = \frac{2}{3}(Q^*)^2 - \frac{1}{\sigma^4} A_{ik} A_{kl} H_{li}^p - \frac{1}{\sigma^4} A_{ik} A_{kl} H_{li}^v, \quad (7)$$

where $\sigma^2 = \langle \text{tr}(\mathbf{S}^2) \rangle$ is the strain variance and $t^* = \sigma t$ is the non-dimensional time. Also, \mathbf{H}^p stands for (minus) the deviatoric part of the pressure Hessian, i.e.,

$$H_{ij}^p = -\left(\frac{\partial^2 p}{\partial x_i \partial x_j} - \frac{\delta_{ij}}{3} \frac{\partial^2 p}{\partial x_k \partial x_k} \right), \quad (8)$$

and $\mathbf{H}^v = \nu \nabla^2 \mathbf{A}$ is the viscous term (recall that in the RE approximation, $\mathbf{H}^p = \mathbf{H}^v = 0$). The Fokker-Planck equation describing the time evolution of the joint density $\mathcal{P}(Q^*, R^*)$ may be written as

$$\frac{\partial \mathcal{P}}{\partial t^*} + \left(\frac{\partial}{\partial Q^*} \right) \cdot \mathcal{W} = 0, \quad (9)$$

where the divergence of the probability current \mathcal{W} controls the time variations of the joint probability density \mathcal{P} .

The probability current can be written in terms of conditional averages as

$$\mathcal{W} = \left\langle \left(\frac{dQ^*}{dt^*} \right) \middle| Q^*, R^* \right\rangle \mathcal{P}(Q^*, R^*) \quad (10)$$

and can be decomposed into $\mathcal{W} = \mathcal{W}_{RE} + \mathcal{W}_p + \mathcal{W}_\nu$, where the probability currents \mathcal{W}_{RE} , \mathcal{W}_p , and \mathcal{W}_ν are associated, respectively, to the effects on the Lagrangian evolution of the invariants Q and R (Eqs. (6) and (7)) of the restricted Euler term $-\mathbf{A}^2$, of (minus) the pressure Hessian $-\mathbf{P}$ and of diffusivity $\nu \nabla^2 \mathbf{A}$ entering in Eq. (1). In this article, we will focus on the probability current associated with the pressure Hessian \mathcal{W}_p . It can be written as

$$\mathcal{W}_p = \left\langle \left(\begin{array}{c} -A_{ik} H_{ki}^p / \sigma^3 \\ -A_{ik} A_{kl} H_{li}^p / \sigma^4 \end{array} \right) \middle| Q^*, R^* \right\rangle \mathcal{P}(Q^*, R^*). \quad (11)$$

More details are provided in Ref. 8.

2. DNS velocity fields

In the following, we will make extensive use of data from standard DNS of the Navier-Stokes equations, for a Taylor-based Reynolds number of order $\mathcal{R}_\lambda = 145$. DNS is based on a pseudo-spectral method with 2nd-order accurate Adams-Bashforth time stepping; the computation box is cubic (size 2π) with periodic boundary conditions in the three directions and spatial resolution 512^3 . Statistical stationarity is maintained by an isotropic external force acting at low wavenumbers in order to ensure a constant energy-

power supply. It provides, in the units of the simulation, a constant energy injection rate $\langle \epsilon \rangle = 0.001$. The kinematic viscosity of the fluid is $\nu = 0.000285$. The Kolmogorov's scale is $\eta_K = (\nu^3 / \langle \epsilon \rangle)^{1/4} = 0.0123$ so that $dx / \eta_K \approx 1$ since $dx = 2\pi / 512$.

We display in Fig. 1(a) the vector plot and streamlines of the probability current \mathcal{W}_p associated with the pressure Hessian (Eq. (11)) in the $R^* Q^*$ -plane, as it was done in Ref. 8. Three main remarks can be made at this stage: (1) first, the pressure Hessian counteracts the development of the finite time singularity along the right tail of the Vieillefosse line implied by the RE term, (2) probabilities are found to be very low in the dissipation production dominated region (i.e., $R^* > 0$ and above the Vieillefosse tail) meaning that pressure does not play there a significant role, and (3) pressure redistributes the probabilities towards the enstrophy production dominated region (i.e., the flux is directed to the left, towards $R^* < 0$). As far as the restricted Euler term is concerned, as is well known,^{1,2} the deterministic \mathcal{W}_{RE} probability current pushes probabilities toward the right tail of the Vieillefosse line (data not shown). This result helps to create a picture of the time evolution of velocity gradients along Lagrangian trajectories in stationary flows: The RE term “pushes” the probabilities towards the right tail towards and along the Vieillefosse line, while the pressure regularizes the implied finite time singularity and redistributes the probabilities towards the left part of the plane such that, in turn, the RE term can act again, etc. To that picture should be added the viscous diffusion effects, \mathcal{W}_ν pushes the probabilities toward vanishing R and Q not only along the Vieillefosse line but also everywhere else, and stochastic forcing, such that the full probability current \mathcal{W} (Eq. (10)) is divergence free, in order to ensure stationary statistics (Eq. (9)).⁸

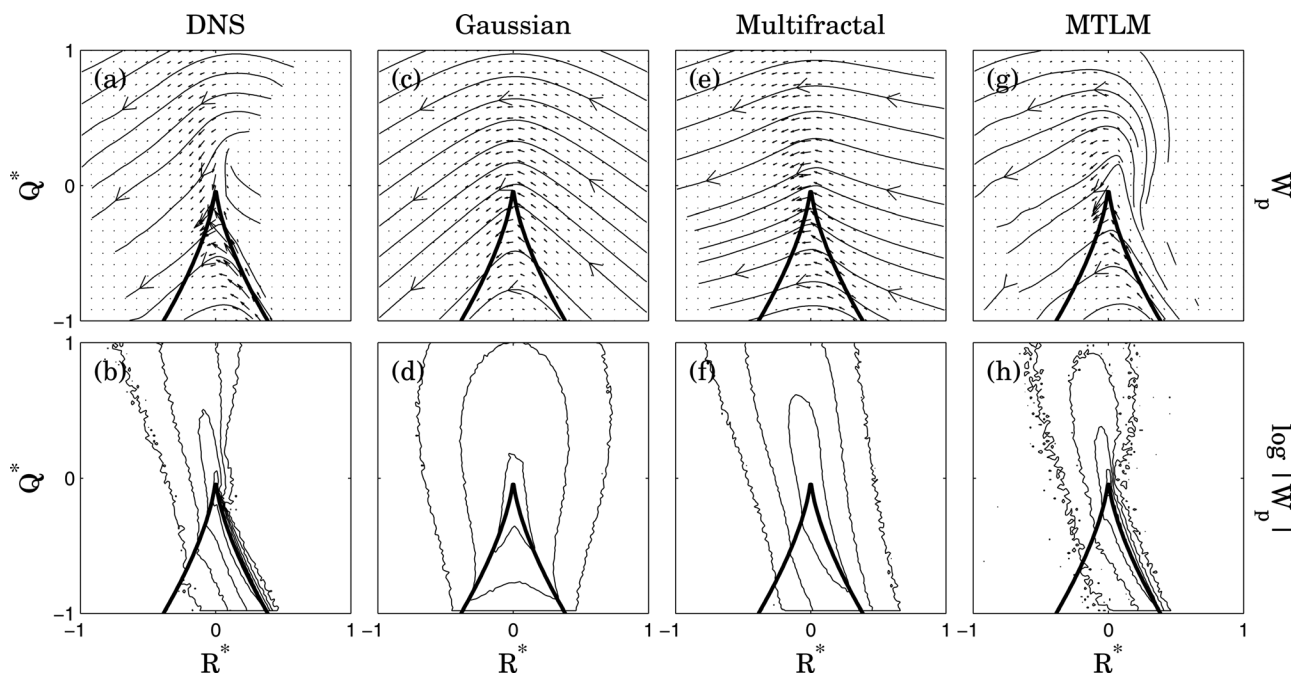


FIG. 1. Probability current \mathcal{W}_p associated with the pressure Hessian—Eq. (11)—for the DNS velocity field and the three synthetic velocity fields—Eqs. (12), (13), and (15)—in the $R^* Q^*$ -plane, where $R^* = R / \langle S_{ij} S_{ij} \rangle^{3/2}$ and $Q^* = Q / \langle S_{ij} S_{ij} \rangle$. The streamlines and vector plots of \mathcal{W}_p are shown in (a,c,e,g). The isoprobability contours of the magnitude of \mathcal{W}_p are shown in (b,d,f,h). Contours are logarithmically spaced by factors of 10, starting at 1 for the contour closest to the origin. The thick lines represent the zero-discriminant (or Vieillefosse) line: $\frac{27}{4} R^2 + Q^3 = 0$.

We display also in Fig. 1(b) the amplitude of \mathcal{W}_p , using logarithmic spacing of iso-probability lines. It can be seen that indeed no current is discernible in the right part of the plane. We remark that it would be interesting to quantify whether the effect of anisotropic pressure Hessian is orthogonal to the RQ -plane in this region, when the RQ plane is extended into three-dimensions, as proposed and studied in Ref. 20.

3. Incompressible Gaussian stochastic velocity field with K41 correlation structure

Let us write a Gaussian homogeneous, isotropic, and incompressible vectorial field $\mathbf{u}(\mathbf{x})$,^{21,22} having a correlation structure consistent with K41 scalings. It reads, in d - dimensions,

$$\mathbf{u}_\epsilon(\mathbf{x}) = \int_{\mathbb{R}^d} \varphi_L(\mathbf{x} - \mathbf{y}) \frac{\mathbf{x} - \mathbf{y}}{|\mathbf{x} - \mathbf{y}|_\epsilon^{\frac{d}{2} + \frac{2}{3}}} \wedge d\mathbf{W}(\mathbf{y}), \quad (12)$$

where $d\mathbf{W}(\mathbf{y}) = (dW_1(\mathbf{y}), dW_2(\mathbf{y}), \dots, dW_d(\mathbf{y}))$ is a Gaussian vectorial white noise and φ_L is a large-scale cut-off which involves the integral length scale L . The deterministic kernel entering into Eq. (12) is regularized over the small length scale ϵ , namely $|\cdot|_\epsilon = \theta_\epsilon^*|\cdot|$ (* stands for the convolution product), with a mollifier $\theta_\epsilon(\mathbf{x}) = \frac{1}{\epsilon^d} \theta(\frac{\mathbf{x}}{\epsilon})$ and $\int \theta(\mathbf{x}) d\mathbf{x} = 1$. It is shown in Ref. 21 that the velocity $\mathbf{u}_\epsilon(\mathbf{x})$ has a well-defined limit when $\epsilon \rightarrow 0$, denoted by $\mathbf{u}(\mathbf{x})$, and such that $\langle |\mathbf{u}(\mathbf{x} + \ell \mathbf{e}) - \mathbf{u}(\mathbf{x})|^q \rangle \sim C_q (\ell/L)^{q/3}$ when $\ell \rightarrow 0$, with C_q a constant independent on the vector \mathbf{e} .

A Gaussian vectorial field, such as from Eq. (12), is a poor representation of turbulence since it does not reproduce several important features such as a mean energy transfer towards small scales (i.e., the skewness phenomenon), the non-Gaussianity of velocity increments (i.e., the intermittency phenomenon), and the alignment of vorticity with the intermediate eigenvector of the strain rate tensor.^{1,3,4} Nevertheless, it is useful to consider it in the analysis of the statistical quantities in which we are interested, such as the probability current \mathcal{W}_p associated with the pressure Hessian (Eq. (11)). In particular, we look at which part can be attributed to Gaussian statistics and which part is really linked to turbulence.

The Gaussian velocity field (Eq. (12)) is computed in a periodic box in $d=3$ space dimensions, using $N = 1024^3$ collocation points. The regularizing parameter ϵ is chosen as $\epsilon = 6dx$, where the spatial resolution is $dx = 1/N$. For the mollifier θ and the large scale cut-off φ , we take Gaussian functions. See Ref. 15 for further numerical details. The Pressure p is defined via the Poisson equation $\Delta p = -\text{tr}(\mathbf{A}^2)$, where \mathbf{A} is the (Gaussian) velocity gradient tensor.

Figure 1(c) shows the vector plot and streamlines of the probability current \mathcal{W}_p obtained from the Gaussian velocity field—Eq. (12). It can be seen that the pressure from the Gaussian field does not counteract directly the singularity along the direction of the right tail of the Vieillefosse line, as is the case in the DNS. Also, there is a significantly higher probability current in the right side region (i.e., $R^* > 0$ and

above the Vieillefosse tail) than in the DNS. The pressure obtained from the Gaussian field is only realistic in the enstrophy production dominated region (i.e., $R^* < 0$), where the behavior shows indeed a trend to push the probability density towards this region. Also, the streamlines cross the $Q = 0$ line meaning that the pressure field from the Gaussian velocity field does produce non-zero effect even when $Q = 0$.

In Fig. 1(d), \mathcal{W}_p -amplitude is shown. It can be seen that the amplitude iso-values are symmetric with respect to the $R^* = 0$ line. We are thus led to the conclusion that a Gaussian velocity field, and its associated pressure field, do not make difference between dissipation production dominated regions ($R^* > 0$) and enstrophy production dominated regions ($R^* < 0$).

4. Incompressible multifractal stochastic velocity field with KO62 statistics

Based on the recent fluid deformation imposed by the Euler flow⁷ and further heuristic introduction of the multifractal structure of turbulence as observed from extensive empirical data (see, e.g., Ref. 16), Ref. 15 proposed the following 3D random vectorial field:

$$\mathbf{u}_\epsilon(\mathbf{x}) = \int_{\mathbb{R}^3} \varphi_L(\mathbf{x} - \mathbf{y}) \frac{\mathbf{x} - \mathbf{y}}{|\mathbf{x} - \mathbf{y}|_\epsilon^{\frac{3}{2} + \frac{2}{3}}} \wedge e^{\mathbf{S}_\epsilon(\mathbf{y})} d\mathbf{W}(\mathbf{y}), \quad (13)$$

where \mathbf{S} is a tensorial Gaussian log-correlated noise of the form,

$$\mathbf{S}_\epsilon(\mathbf{y}) = \sqrt{\frac{5}{4\pi}} \lambda \int_{|\mathbf{y} - \boldsymbol{\sigma}| \leq L} \left[\frac{(\mathbf{y} - \boldsymbol{\sigma}) \otimes [(\mathbf{y} - \boldsymbol{\sigma}) \wedge d\mathbf{W}(\boldsymbol{\sigma})]}{|\mathbf{y} - \boldsymbol{\sigma}|_\epsilon^{7/2}} + \frac{[(\mathbf{y} - \boldsymbol{\sigma}) \wedge d\mathbf{W}(\boldsymbol{\sigma})] \otimes (\mathbf{y} - \boldsymbol{\sigma})}{|\mathbf{y} - \boldsymbol{\sigma}|_\epsilon^{7/2}} \right], \quad (14)$$

with \otimes denoting the tensorial product. The form of the symmetric matrix \mathbf{S}_ϵ is inspired by the recent fluid deformation closure experienced by the fluid over short times,¹⁵ and the exponent $7/2$ has been selected such that the components of \mathbf{S} are correlated logarithmically in space. A free parameter λ enters this construction and governs the level of intermittency of the field. We will take in the sequel $\lambda^2 = 0.025$ in order to be consistent with empirical findings.²³

Generation of the vectorial field $\mathbf{u}_\epsilon(\mathbf{x})$ can be done accurately and efficiently in periodic boxes using up to 1024^3 collocation points, in a similar way as done for the Gaussian velocity field (Eq. (12)). The cost of the computation of the matrix exponential is the limiting numerical step. It is estimated at each point of space using a Padé approximant with scaling and squaring (see Ref. 15 for details).

It has been shown numerically (Ref. 15) that the multifractal velocity field—Eq. (13)—gives a realistic representation of instantaneous realizations of velocity fields in fully developed turbulence in the inertial range in regard to the following properties: (1) Longitudinal $\delta_\ell u$ and transverse velocity increments are intermittent, λ being the intermittency coefficient, (2) the third-order moment $\langle (\delta_\ell u)^3 \rangle$ is negative and proportional to the scale ℓ . The fact that there is negative

skewness $S = \langle (\delta_\ell u)^3 \rangle / \langle (\delta_\ell u)^2 \rangle^{3/2}$ means that \mathbf{u} exhibits a non-vanishing mean energy transfer towards the small scales, and (3) vorticity gets preferentially aligned with the eigenvector of the strain-rate tensor corresponding to the intermediate eigenvalue.

We show in Fig. 1(e) the vector plot and streamlines of the probability current \mathcal{W}_p obtained from the multifractal velocity field. It can be seen that, in a similar fashion to the Gaussian case, streamlines are roughly symmetric with respect to the $R^* = 0$ line. This is not consistent with DNS in the $R^* > 0$ region, but it is still realistic in the $R^* < 0$ region. The difference with the Gaussian field is the fact that now the joint density of R^* and Q^* is not symmetric with respect to the $R^* = 0$ line, showing thus the predominance of the regions for enstrophy-enstrophy production (upper-left quadrant, which in turbulent flows is correlated with vortex stretching) and dissipation-dissipation production (lower-right quadrant, connected with biaxial straining in turbulent flows). This is also the case for the probability current amplitude, as shown in Fig. 1(f). We can see, therefore, that both the Gaussian and multifractal velocity fields do not reproduce the void in probability in the $R^* > 0$ region as observed in DNS, but they do reproduce accurately the probability current evolutions in the $R^* < 0$ regions and the presence of probability flux at $Q = 0$.

5. MTLM velocity field

We consider a third case of a synthetic velocity field. The minimal turnover Lagrangian map (MTLM) velocity field is obtained by distorting an initially random solenoidal vector field, $\mathbf{u}_0(\mathbf{x})$, over a hierarchy of spatial scales $\{\ell_n = 2^{-n}L, n = 1, \dots, M\}$, where L is of the order of the integral scale and the smallest scale, ℓ_M , is in the order of Kolmogorov scale. This generates the multiscale recursive sequence,

$$\mathbf{u}_n(\mathbf{x}) = T[\mathbf{u}_{n-1}(\mathbf{x}), \ell_n] \quad n = 1, \dots, M, \quad (15)$$

whose final step, $\mathbf{u}_M(\mathbf{x})$, is the synthetic velocity field. Here, $T[\cdot]$ stands for the distortion operations applied. At each level n in the sequence, the velocity is filtered at scale ℓ_n and decomposed into low-pass and high-pass filtered parts: $\mathbf{u}^<$ and $\mathbf{u}^>$, respectively. The $\mathbf{u}^<$ part is deformed by mapping the velocity vectors from their collocation points, \mathbf{x} , to new positions that fluid particles moving at constant velocity in Lagrangian coordinates would reach: $\mathbf{u}^<(\mathbf{X}(t), t) = \mathbf{u}^<(\mathbf{x}, 0)$, with $\mathbf{X}(t) = \mathbf{x} + t\mathbf{u}^<(\mathbf{x})$. The parameter t is taken equal to the eddy-turnover time-scale corresponding to the spatial scale ℓ_n , computed using standard Kolmogorov scaling. New velocity values at the collocation points are obtained by interpolation over nearby velocities that have come into a neighborhood of radius ℓ_n around \mathbf{x} after the mapping. This deformed field $\mathbf{u}^<$ is made solenoidal again by projection in Fourier space, and the amplitudes of its Fourier modes are scaled to conform to the target energy spectrum. Finally, $\mathbf{u}^<$ is recombined with the $\mathbf{u}^>$ part, which at this stage still remains as a Gaussian field.

The next generation in the hierarchy will take the complete field \mathbf{u} and will apply the same distortion operations,

now with the field decomposed at a smaller filtering scale. In this way, the effects are superposed and accumulated over a range of spatial scales. Further details and characteristics of these synthetic velocity fields can be found in Refs. 17 and 18. The present MTLM velocity field was generated in a periodic box, using 512^3 collocation points, with $M = 6$ generations in the hierarchy, and an energy spectrum corresponding to $\mathcal{R}_\lambda \approx 250$.

The results for the probability current \mathcal{W}_p obtained from the MTLM velocity field (Eq. (15)) are shown in Figs. 1(e) and 1(f). When compared with the DNS results (Figs. 1(a) and 1(b)), we can see a close agreement of both magnitude and direction of \mathcal{W}_p . In particular, the MTLM velocity field reproduces, for pressure-related part of the probability current, the void of probability in the $R^* > 0$ region. We can conclude that, of the three cases studied, the MTLM velocity field gives the most realistic synthetic turbulence, as far as anisotropic pressure Hessian effects are concerned. But some small difference can be observed in the $R^* > 0$ region, close to the origin, where the MTLM fields seem to predict a circular motion that is not present in DNS.

B. Mean pressure Hessian norm conditioned on Q

As previously noticed in Ref. 8, current closures for the pressure Hessian^{5,7,14} are proportional to the invariant Q . This is in particular the case for the closure provided in Ref. 7, namely

$$\mathbf{P} = -\frac{\mathbf{C}_{\tau_\eta}^{-1}}{\text{tr}(\mathbf{C}_{\tau_\eta}^{-1})} \text{tr}(\mathbf{A}^2), \quad (16)$$

where \mathbf{C}_{τ_η} is the statistically stationary Cauchy-Green tensor at the Kolmogorov time scale τ_η (Refs. 7 and 8) and $\text{tr}(\mathbf{A}^2) = -2Q$. Indeed, it is tempting to close the anisotropic part of \mathbf{P} as a symmetric tensor proportional to Q since the isotropic part is itself proportional to Q as seen on the Poisson equation $\Delta p = 2Q$. It would imply in particular that the probability current \mathcal{W}_p vanishes on the $Q = 0$ line. This is not observed on DNS (see Figs. 1(a) and 1(b)). To quantify more precisely the behavior of \mathbf{P} in the neighborhood of vanishing Q , we proposed in Ref. 8 to estimate the average pressure Hessian (square) norm $|\mathbf{P}|^2 = \text{tr}(\mathbf{P}^2)$ conditioned on the invariant Q . The corresponding conditional average $\langle \text{tr}(\mathbf{P}^2) | Q \rangle$ was shown for fields obtained by DNS as well as by applying the closure (Eq. (16)). It was observed that for the DNS case, such conditional average at $Q = 0$ does not vanish and, furthermore, it behaves nearly linearly with Q , whereas the closure Eq. (16) predicts a vanishing conditional average for $Q = 0$ and a quadratic behavior with Q .

We display in Fig. 2 the conditional average $\langle \text{tr}(\mathbf{P}^2) | Q \rangle$ as a function of Q for the four different velocity fields: the DNS, Gaussian (Eq. (12)), multifractal (Eq. (13)), and MTLM (Eq. (15)) velocity fields. As previously observed, for the DNS case (solid line), the conditional average does not vanish at $Q = 0$ and behaves linearly with Q in the neighborhood around $Q = 0$. For all the three remaining synthetic velocity fields, the conditional average does not vanish at $Q = 0$ and, hence, they perform better than the deterministic

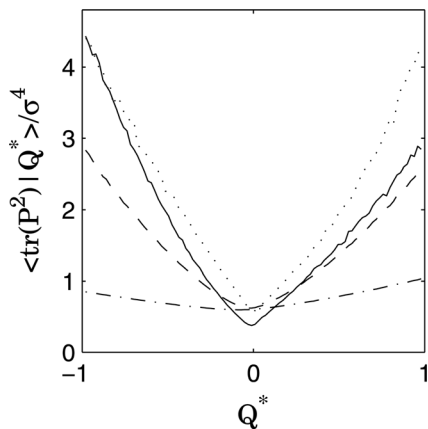


FIG. 2. Conditional expectation $\langle \text{tr}(\mathbf{P}^2) | Q^* \rangle$ of pressure Hessian norm on Q^* : DNS (solid line), Gaussian (dotted-dashed line), multifractal (dashed line), and MTLM (dotted line) velocity fields.

closure (Eq. (16)) on this issue. For the Gaussian case, however (dash-dotted line), the tails of the conditional average are not realistic, being far below the curves corresponding to the DNS case. Numerical simulations of the Gaussian fields at lower resolutions, i.e., $N=256^3$ or $N=512^3$ (data not shown), showed no difference with the $N=1024^3$ case. Interestingly, in this regard, the multifractal field (dashed line) performed much better, exhibiting conditional average tails very close to the DNS result. Some discrepancy is found for negative Q s, where the tail in the DNS case has a steeper slope. The MTLM velocity field (dotted line) also performs well against DNS data, although its tails are found to be quite symmetric, at odds with DNS.

Overall, the behavior of the pressure Hessian obtained from the three synthetic velocity fields is reasonably satisfactory when compared against DNS data. The probability current is well reproduced in the $R < 0$ region and the conditional average shown in Fig. 2 does not vanish for vanishing Q . Only the MTLM velocity field can reproduce additionally the void in probability observed in DNS over the $R^* > 0$ region (explaining, or at least giving an interpretation of the lack of action of the pressure Hessian in the dissipation production dominated region $R^* > 0$ remains, however, an open problem). Furthermore, we have shown that synthetic velocity fields do predict the pressure Hessian square norm as being closer to linearly proportional to the invariant Q , rather than proportional to Q^2 as is the case in existing closures, in particular Eq. (16).

At this stage, one could reach the conclusion that some approximate surrogates of an actual turbulent field, even when obtained with the simplest Gaussian approximation, contain a better prediction of the behavior of the pressure Hessian, in connection with its dependence on Q , than the deterministic closure given by Eq. (16). We will see in the following that the anisotropic part of the pressure Hessian can, in fact, be accurately closed by the local spatial variations of the invariant Q .

III. LOCALITY OF THE PRESSURE HESSIAN

We have seen in the first part of this work that a simple Gaussian approximation, given by Eq. (12), or more sophisti-

cated synthetic velocity fields, such as Eqs. (13) and (15), can reproduce the motion of the probability current \mathcal{W}_p associated with the pressure Hessian in the $R^* < 0$ region. Additionally, taking into account the spatial distribution of the velocity field also leads to a non-vanishing conditional mean pressure Hessian norm for $Q=0$. In this section, we study to what degree spatial locality is important in determining these properties of the anisotropic part of the pressure Hessian.

The exact expression (2) for the pressure Hessian is very useful since it allows interpreting its isotropic part as being local, whereas the anisotropic part is governed by $\text{tr}(\mathbf{A}^2)$, or equivalently Q at different locations, i.e., it contains non-local contributions from the spatial variations of Q . In this section, we will work with an equivalent form of Eq. (2) that underlines the role played by the Hessian \mathbf{Q} of the invariant Q . Indeed, taking two spatial derivatives of the Poisson equation that commute with the Laplacian, one obtains $\Delta \mathbf{P} = 2\mathbf{Q}$, where $Q_{ij} = \frac{\partial^2 Q}{\partial x_i \partial x_j}$. It is then easily seen that a similar relation exists between the deviatoric parts of \mathbf{P} and \mathbf{Q} , namely $\Delta \mathbf{P}^d = 2\mathbf{Q}^d$, where the superscript d denotes the deviatoric part, i.e., for example, $\mathbf{P}^d = \mathbf{P} - \frac{1}{3}\text{tr}(\mathbf{P})\mathbf{I}$, with \mathbf{I} being the identity matrix. We finally reach a relation, equivalent to Eq. (2), between \mathbf{P}^d and \mathbf{Q}^d

$$\mathbf{P}^d(\mathbf{x}) = -\frac{1}{2\pi} \int \frac{1}{|\mathbf{x} - \mathbf{y}|} \mathbf{Q}^d(\mathbf{y}) d\mathbf{y}. \quad (17)$$

Relation (17) is exact. In the following, we will truncate the integral present in Eq. (17) over a ball, centered at \mathbf{x} , and of radius η , namely

$$\mathbf{P}^d(\mathbf{x}) \approx -\frac{1}{2\pi} \int_{|\mathbf{x} - \mathbf{y}| \leq \eta} \frac{1}{|\mathbf{x} - \mathbf{y}|} \mathbf{Q}^d(\mathbf{y}) d\mathbf{y}. \quad (18)$$

It is easily seen that from Eq. (18), we recover Eq. (17) by taking $\eta \rightarrow +\infty$. We now make the strong assumption that η is of order of the Kolmogorov length scale η_K . In this case, we can Taylor-expand the Hessian of Q at the position \mathbf{y} around its value at the location \mathbf{x} , take out $\mathbf{Q}^d(\mathbf{x})$ from the integral, and perform the remaining integration in spherical coordinates. We get an expression for the deviatoric part of the pressure Hessian,

$$\left(\frac{\partial^2 p}{\partial x_i \partial x_j} \right)^d \approx -\eta^2 \left(\frac{\partial^2 Q}{\partial x_i \partial x_j} \right)^d. \quad (19)$$

This now expresses the anisotropic part of the pressure Hessian in terms of local properties of the invariant Q , although the latter's spatial derivatives are needed. These derivatives are unknown in the closure and Lagrangian models of, e.g., Ref. 7, and so this does not constitute a practical closure yet. To ensure that this expression yields the same norm as the true pressure Hessian, we define the ball's radius according to

$$\eta^2 = \sqrt{\frac{\langle \text{tr}(\mathbf{P}^2) \rangle}{\langle \text{tr}(\mathbf{Q}^2) \rangle}}. \quad (20)$$

The expression (19) and the choice of the length scale η by Eq. (20) are consistent only if (1) eigenvalues and

eigenvectors of \mathbf{P}^d and \mathbf{Q}^d are well correlated and (2) η is indeed of the order of the Kolmogorov length scale η_K since we assume that in the neighborhood of \mathbf{x} , $\mathbf{Q}^d(\mathbf{y}) \approx \mathbf{Q}^d(\mathbf{x})$.

Both Hessian tensors, for the pressure and for Q , are computed in Fourier space, for the periodic DNS flows. The expression (19) requires the computation of the second derivative of Q , which is already the square of a first spatial derivative. This is a reason for our use of the highly resolved DNS under study, in which $dx/\eta_K \approx 1$ (see Sec. II A 2). Using $\eta_K = (\nu^3/\langle \epsilon \rangle)^{1/4} = 0.0123$, we find that for the current DNS, our choice of the length scale η as Eq. (20) implies that $\eta = 1.83 \eta_K$. Hence, η is of the order of η_K , as required. Let us stress that a well resolved DNS is necessary since some noise can be introduced by the computation of third order derivatives, leading to a bad estimation of the parameter η . More work is needed to clarify this point and to assess the dependence of η on resolution effects and Reynolds numbers. This could be done, for example, performing specifically designed DNS aimed at quantifying accurately high-order velocity derivatives, as was proposed in Refs. 24 and 25.

We display in Fig. 3 the joint probability densities of the three eigenvalues of the deviatoric part of the true pressure Hessian (denoted by λ_p) and the corresponding eigenvalues of the expression $-\eta^2 \mathbf{Q}^d$ (denoted by λ_q). The smallest (Fig. 3(a)) and largest eigenvalues (Fig. 3(c)) are found to be well correlated with joint density contours that are elongated along the perfect correlation line (i.e., $\lambda_p = \lambda_q$) and correlation coefficients of $\rho = 0.714$ and $\rho = 0.703$, respectively.

As far as the intermediate eigenvalue is concerned, weaker correlation is found ($\rho = 0.275$), with isolines being close to circles. We can conclude that the smallest and larg-

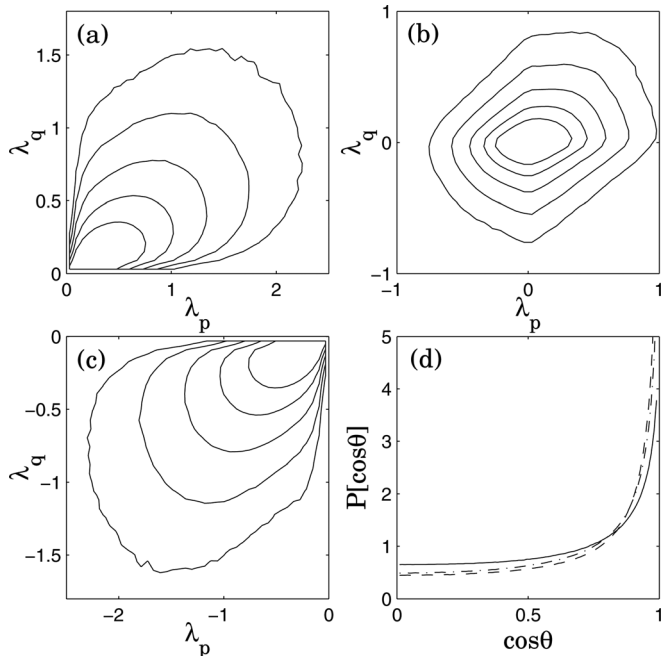


FIG. 3. In (a,b,c), we show the joint PDF of eigenvalues λ_p of the pressure Hessian and eigenvalues λ_q of the proposed local expression (Eq. (19)). Iso-probability lines correspond to e^{-4} , e^{-3} , e^{-2} , e^{-1} , 1. In (d) is shown the PDF of the cosine of the angle between the eigenvectors of \mathbf{P} and those of the local closure (Eq. (19)): eigenvectors associated to the smallest (dashed), intermediate (solid), and biggest (dot-dashed) eigenvalues.

est eigenvalues are well correlated. In Fig. 3(d), we display the probability of the cosine of the angle between the eigenvectors of the left and right terms of Eq. (19). It is found that in all the cases, corresponding to the three different eigenvalues, the maximum of probability is reached when the eigenvectors of \mathbf{P}^d and $-\eta^2 \mathbf{Q}^d$ are aligned. These results show then that \mathbf{P}^d and $-\eta^2 \mathbf{Q}^d$ are correlated both in amplitude and eigendirections. We have seen that, in tensorial structure, the true pressure Hessian \mathbf{P}^d and the local expression in terms of velocity gradients $-\eta^2 \mathbf{Q}^d$ are quite similar. We may now wonder if the local expression is able to reproduce the probability current associated to pressure effects as seen in Figs. 1(a) and 1(b). To this purpose, we show in Figs. 4(a) and 4(b) the probability current \mathcal{W}_p obtained from DNS when the true pressure Hessian is replaced by the local expression (19). We see in Fig. 1(a) that, indeed, the local expression reproduces the counteractive action of the pressure along the right tail of the Vieillefosse line. Furthermore, a void in probability is found in dissipation production dominated regions (i.e., $R^* > 0$), as can be clearly seen in Fig. 1(b). Finally, the local expression also reproduces some of the probability redistribution in the enstrophy production dominated region ($R^* < 0$), as observed in DNS (Figs. 1(a) and 1(b)), although the direction of the probability flux streamlines for $R^* < 0$ is seen to be more vertical than the leftwards directions seen in the DNS. Also, the streamlines are found more curved for the local expression than for \mathbf{P} , and the probability current amplitude $|\mathcal{W}_p|$ is found to decrease faster at high values of R and Q than in the DNS case. This could be due to limitations of the localized expression in reproducing very high turbulent fluctuations.

The overall behavior of the local expression in the RQ -plane is on the whole quite satisfactory when compared against DNS. Some differences appear: (1) the streamlines of the probability current are found more curved for the local closure than for \mathbf{P} , very much in opposition to the streamlines imposed by the RE approximation (see Ref. 8) and (2) the probability current amplitude $|\mathcal{W}_p|$ is found to decrease faster at high values of R and Q than in the DNS case. This could be due to limitations of the localized expression in reproducing very high turbulent fluctuations. On the whole, however, the trends provided by the local expression Eq. (19) agree quite well compared to the DNS results in terms of the probability fluxes in the RQ plane.

We also show in Fig. 4(c) the conditional expectation of the pressure Hessian square norm, based on Q . For the sake of clarity, we show again the conditional average as obtained in DNS (solid line) (it was already shown in Fig. 2). We use open symbols (\circ) to show the conditional expectation obtained from DNS using the local approximation (19). It can be seen that the conditional expectation obtained from the local approximation is in very good agreement with the DNS, with some discrepancies appearing for negative Q^* . Interestingly, we see that the conditional expectation does not vanish for $Q = 0$. This is consistent with former remarks made about the requirement that a realistic model of \mathbf{P} cannot be simply proportional to Q .

Finally, to quantify the agreement between individual tensor elements, we show in Fig. 4(d) the joint Probability

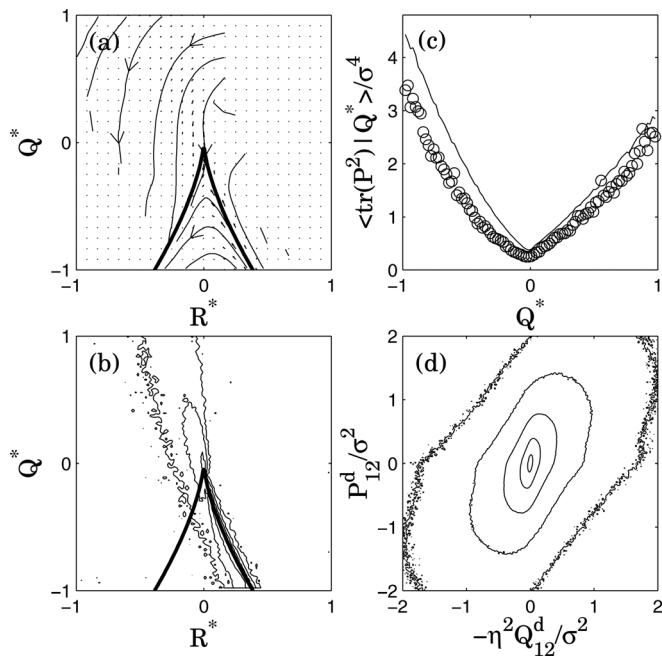


FIG. 4. (a) and (b): Probability current \mathcal{W}_p associated with pressure Hessian (Eq. (11)) for the DNS velocity field when using the local closure (19). See Fig. 1 for further details. (c) Conditional expectation $\langle \text{tr}(\mathbf{P}^2) | Q \rangle$ of pressure Hessian norm on Q^* : DNS (solid) and closure (\circ), in a similar fashion than in Fig. 2. (d) Joint PDF of the components P_{12} and $-\eta^2 Q_{12}$ in a logarithmic scale. Isolines correspond to probability $[10^{-3}, 10^{-2}, 10^{-1}, 1, 10]$.

Density Function (PDF) of the component P_{12} and the component $-\eta^2 Q_{12}$. This plot demonstrates the good level of correlation between these two tensors since the joint PDF is clearly elongated along the perfect correlation line (i.e., $P_{12} = -\eta^2 Q_{12}$). The corresponding correlation coefficient is $\rho = 0.55$. Thus, also this statistical test confirms the good agreement between the local approximation and the true pressure Hessian.

IV. CONCLUSIONS AND PERSPECTIVES

This article focuses on the statistical nature of the pressure Hessian that governs much of the Lagrangian dynamics of the velocity gradient tensor in turbulence. In the first part, we have seen that synthetic velocity fields reproduce many properties of the pressure Hessian as they are seen in DNS flows, such as the non-trivial behavior of the probability current, and the conditional expectation of the pressure Hessian norm on the invariant Q . Even the simplest Gaussian approximation for the velocity field (Eq. (12)) can represent some non-trivial behaviors of the pressure that could not be predicted by the closures in terms of \mathbf{A} .^{5,7,14} Based on this observation and on an exact field description of the pressure Hessian by means of nonlocal integrals (Eqs. (2) and (17)), we formulate the hypothesis that considering only the integration over a ball of radius η_K and neglecting other contributions, the deviatoric part of \mathbf{P} could be expressed in terms of local properties of the velocity gradient tensor, but in terms of higher-order derivatives. Specifically, the spatially local approximation is not expressed in terms of \mathbf{A} , but in terms of second-order derivatives of Q . This approximation was found to be highly correlated with the true pressure Hes-

sian \mathbf{P} when compared in DNS computations. These findings show that the main contribution to $\mathbf{P}(\mathbf{x})$ is contained in the local neighborhood around position \mathbf{x} , in a ball centered at \mathbf{x} , and of radius of the order of η_K . This raises the hope that local closures involving a finite set of ordinary differential equations may still be possible for studying the Lagrangian dynamics of the velocity gradient tensor. To that end, it is still necessary to express the Hessian of Q in terms of the local values of \mathbf{A} . Only then would we have a full closure.

Let us finally remark that if a tractable transport equation for the pressure Hessian is difficult to get, the Lagrangian derivatives of p and \mathbf{P} can be related. We get the following transport equation for the pressure Hessian:

$$\frac{d^O \mathbf{P}}{dt} = -\frac{\partial p}{\partial x_k} \nabla \nabla u_k + \nabla \nabla \frac{dp}{dt}, \quad (21)$$

where d^O/dt stands for the upper convected time derivative or Oldroyd derivative that relates the rate of change written in the coordinate system rotating and stretching with the fluid (see, for example, Ref. 26), i.e.,

$$\frac{d^O \mathbf{P}}{dt} = \frac{d\mathbf{P}}{dt} + \mathbf{A}^\top \mathbf{P} + \mathbf{P} \mathbf{A}. \quad (22)$$

Then, if we neglect the right-hand side of Eq. (21) in the rate of change of the pressure Hessian, i.e., if we assume that the Oldroyd derivative (22) vanishes, and we apply the recent fluid deformation (RFD) approximation (assuming \mathbf{A} independent on time), we get that for an early time

$$\mathbf{P}(\tau) = e^{-\tau \mathbf{A}^\top} \mathbf{P}(0) e^{-\tau \mathbf{A}}. \quad (23)$$

This remark justifies the use of matrix exponentials as closures of the pressure Hessian,⁷ as it was also noted for the subgrid-scale stress tensor.²⁷ If in addition we start from an initial isotropic pressure Hessian, and include the Poisson equation, we recover exactly the closure (16) proposed in Ref. 7. This represents useful perspectives for future investigations on the Lagrangian dynamics of the velocity gradient tensor.

ACKNOWLEDGMENTS

We thank G. Eyink and B. Lüthi for fruitful discussions. We acknowledge the Leonardo Da Vinci Programme for support in the internship of F.T. at the ENS, and the CNRS for constant support. DNS and stochastic fields have been performed by using the local computing facilities (PSMN) at ENS Lyon under grant CPER-CIRA. This research was supported in part by the National Science Foundation under Grant No. NSF PHY05-51164 during the stay of L.C. at the KITP (Santa Barbara). C.M. and H.Y. are supported by NSF Grant No. CDI-0941530. C.R. acknowledges the support of CONICYT under Project Fondecyt 11080025.

¹C. Meneveau, "Lagrangian dynamics and models of the velocity gradient tensor in turbulent flows," *Annu. Rev. Fluid Mech.* **43**, 219 (2011).

²B. J. Cantwell, "Exact solution of a restricted Euler equation for the velocity gradient tensor," *Phys. Fluids A* **4**, 782 (1992).

³A. Tsinober, *An Informal Introduction to Turbulence* (Kluwer Academic, Dordrecht, 2001).

- ⁴J. M. Wallace, "Twenty years of experimental and direct numerical simulation access to the velocity gradient tensor: What have we learned about turbulence?," *Phys. Fluids* **21**, 021301 (2009).
- ⁵M. Chertkov, A. Pumir, and B. I. Shraiman, "Lagrangian tetrad dynamics and the phenomenology of turbulence," *Phys. Fluids* **11**, 2394 (1999).
- ⁶E. Jeong and S. S. Girimaji, "Velocity-gradient dynamics in turbulence: Effect of viscosity and forcing," *Theor. Comput. Fluid Dyn.* **16**, 421 (2003).
- ⁷L. Chevillard and C. Meneveau, "Lagrangian dynamics and statistical geometric structure of turbulence," *Phys. Rev. Lett.* **97**, 174501 (2006).
- ⁸L. Chevillard, C. Meneveau, L. Biferale, and F. Toschi, "Modeling the pressure Hessian and viscous Laplacian in turbulence: Comparisons with DNS and implications on velocity gradients dynamics," *Phys. Fluids* **20**, 101504 (2008).
- ⁹K. Ohkitani, "Eigenvalue problems in three-dimensional Euler flows," *Phys. Fluids A* **5**, 2570 (1993).
- ¹⁰P. Constantin, "Geometric statistics in turbulence," *SIAM Rev.* **36**, 73 (1994).
- ¹¹K. Ohkitani and S. Kishiba, "Nonlocal nature of vortex stretching in an inviscid fluid," *Phys. Fluids A* **7**, 411 (1995).
- ¹²A. Majda and A. Bertozzi, *Vorticity and Incompressible Flow* (Cambridge University, Cambridge, 2002).
- ¹³K. Ohkitani, "A miscellany of basic issues on incompressible fluid equations," *Nonlinearity* **21**, T255 (2008).
- ¹⁴J. D. Gibbon and D. D. Holm, "Lagrangian particle paths and orthonormal quaternion frames," *Nonlinearity* **20**, 1745 (2007).
- ¹⁵L. Chevillard, R. Robert, and V. Vargas, "A stochastic representation of the local structure of turbulence," *Europhys. Lett.* **89**, 54002 (2010).
- ¹⁶U. Frisch, *Turbulence* (Cambridge University, Cambridge, 1995).
- ¹⁷C. Rosales and C. Meneveau, "A minimal multiscale Lagrangian map approach to synthesize non-Gaussian turbulent vector fields," *Phys. Fluids* **18**, 075104 (2006).
- ¹⁸C. Rosales and C. Meneveau, "Anomalous scaling and intermittency in three-dimensional synthetic turbulence," *Phys. Rev. E* **78**, 016313 (2008).
- ¹⁹F. van der Bos, B. Tao, C. Meneveau, and J. Katz, "Effects of small-scale turbulent motions on the filtered velocity gradient tensor as deduced from holographic PIV measurements," *Phys. Fluids* **14**, 2457 (2002).
- ²⁰B. Lüthi, M. Holzner, and A. Tsinober, "Expanding the QR space to three dimensions," *J. Fluid Mech.* **641**, 497 (2009).
- ²¹R. Robert and V. Vargas, "Hydrodynamic turbulence and intermittent random fields," *Commun. Math. Phys.* **284**, 649 (2008).
- ²²P. D. Tafti and M. Unser, "Fractional Brownian vector fields," *Multiscale Model. Simul.* **8**, 1645 (2010).
- ²³L. Chevillard, B. Castaing, E. Lévêque, and A. Arneodo, "Unified multifractal description of velocity increments statistics in turbulence: Intermittency and skewness," *Physica D* **218**, 77 (2006).
- ²⁴Z.-S. She, S. Chen, G. Doolen, R. H. Kraichnan, and S. A. Orszag, "Reynolds number dependence of isotropic Navier-Stokes turbulence," *Phys. Rev. Lett.* **70**, 3251 (1993).
- ²⁵J. Schumacher, "Sub-Kolmogorov-scale fluctuations in fluid turbulence," *Europhys. Lett.* **80**, 54001 (2007).
- ²⁶P. Haupt, *Continuum Mechanics and Theory of Materials* (Springer, Berlin, 2000).
- ²⁷Y. Li, L. Chevillard, G. Eyink, and C. Meneveau, "Matrix exponential-based closures for the turbulent subgrid-scale stress tensor," *Phys. Rev. E* **79**, 016305 (2009).